Search for Double Partons at CDF

Lee Pondrom[∗] **for the CDF Collaboration**
*University of Wisconsin, Madison*
E-mail: pondrom@fnal.gov

A search for double parton hard scattering has been performed using the $Z \rightarrow \mu^+ \mu^-$ sample of the CDF detector corresponding to $9 fb^{-1}$ of $\bar{p}p$ collision data taken in Run 2 at 1.96 TeV. The transverse region in ϕ relative to p_{TZ}, defining the 'underlying event', is used to look for a jet pair from a second hard scatter. No back-to-back dijet excess is seen in 45,633 Z events with $p_{TZ} > 10$ GeV/c and at least one jet with $E_T > 5$ GeV.

[∗]Speaker.
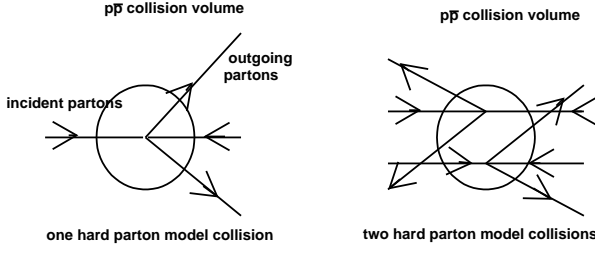
**Figure 1:** Schematic diagrams of single parton (left) and double parton (right)scattering in the same p̄p collision.

1. Introduction

The CDF collaboration has published a study of the 'underlying event' in the $Z \to l^+l^-$ data produced by p̄p collisions at 1.96 TeV. [1] A result of this study is a tune of the Monte Carlo simulation program PYTHIA [2] to reproduce the observed underlying event activity. The number of secondary or rescattering non-perturbative interactions is one of the parameters adjusted in the tune.

Double parton interactions are a natural extension of the parton model. The parton model is an essential ingredient of Monte Carlo simulation programs like PYTHIA, and has enjoyed much success in describing high energy hadron collisions as parton-parton $2 \to 2$ scattering folded into parton distributions determined by lepton-hadron scattering. In a double parton interaction this process occurs twice in the same p̄p collision. Figure 1 shows schematically the single and double parton processes. The two hard scatters are perturbative, and are independent, consistent with the conservation laws. If the momentum fractions and energies involved in the two scatters are modest, independence should obtain. Therefore, a second $2 \to 2$ scatter resulting in two back to back jets in the final state independent of the primary interation is a signature of double parton interactions (DPI). Such a process can be modeled by two separate interactions (vertices) in the same event. A recent study by the D0 Collaboration reviews previous work in this subject. [3]

2. Apparatus

The CDF Run 2 detector has been described elsewhere [4]. Vital components of the CDF detector for this analysis were the central charged particle tracker, called the COT, the central electromagnetic and hadronic calorimetry, called CEM and CHA respectively, and the central muon detectors. The origin of the right-handed CDF coordinate system was at the center of the detector, on the beam line, with $\hat{z}$ in the proton direction, $\hat{x}$ in the horizontal plane, and $\hat{y}$ directed vertically upwards. The azimuthal angle ϕ was measured in the xy plane, and the polar angle θ was used to define the pseudorapidity $\eta = -\log(\tan(\theta/2))$. Events were restricted to the central region ($|\eta| < 1$), where the tracking efficiency was high. The COT was a drift chamber in a 1.4 T magnetic field parallel to $\hat{z}$, with an inner radius of 40 cm and an outer radius of 140 cm, containing 30,000 sense wires. The single charged track momentum resolution, including the vertex constraint in the
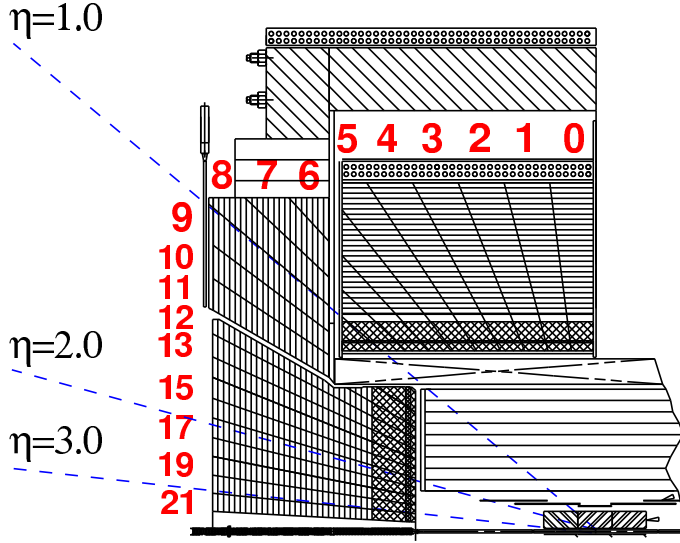
Figure 2: CDF calorimetry tower configuration. Towers 0-5 are in the CHA; towers 6 and 7 are shared between the CHA and the WHA (endwall); towers 8-11 are WHA, and 21-21 are PHA (Plug).The CMU muon chambers are just outside the CHA, inside the return iron, while the CMP chambers are outside the return iron.

xy plane, was $\delta p_T/p_T^2 = 0.001 (\text{GeV/c})^{-1}$, or $\delta p_T/p_T = 0.05$ at 50 GeV/c. The z vertex resolution for an extrapolated COT track was $\delta z = 3$ mm.

The CEM and the CHA were sampling calorimeters, with lead plates and iron plates respectively, interspersed with scintillator. The CEM had 31 lead plates each 0.32 cm thick, and 0.5 cm scintillator, for a total of 18 radiation lengths, while the CHA had 32 iron plates each 2.5 cm thick, and 1.0 cm scintillator. The total number of interaction lengths for pions penetrating the CEM+CHA was 5.5, a number relevant both for hadronic energy resolution and muon detection. The calorimeters were arranged in towers in (η, ϕ) space, with granularity $\delta \eta = 0.1$ and $\delta \phi = 0.26(15^0)$. A side view of 1/4 of the tracking and calorimetry is shown in figure 2. The energy resolution at 50 GeV (σ/E) for CEM was 2%, and for CHA was 11%. The measured transverse energies were corrected using the standard jet energy corrections package. [5].

The central muon detectors had two components, called the CMU and the CMP. CMU was composed of a barrel of 4.52 m long drift chambers outside the central calorimeters, 3.5 m radial distance from the beam line, covering ± 0.6 in η.To increase the absorber and improve the pion rejection a second set of drift chambers was installed outside the 60 cm thick iron return yoke on the top and bottom of the detector. Drift chambers were also installed on the sides of the detector, outside extra 60 cm thick iron plates. Muon candidates with tracks in the CMP traversed about 7.8 pion interaction lengths. The CMP was a square box outside the detector, with η coverage matching the CMU. A good quality central muon candidate had momentum measured in the COT, and matched drift chamber stubs in both the CMU and CMP. Such muon candidates had negligible background.
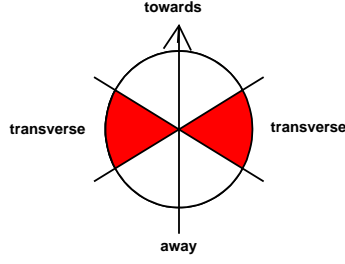
3. Transverse tracks

The transverse region in the ϕ plane perpendicular to the beams is defined by $\pi/3 < \Delta\phi < 2\pi/3$ relative to the highest E_T jet in the jet data sample, or p_{TZ} in the Drell-Yan sample with $Z \to \mu^+\mu^-$, as shown in figure 3. Figure 4 shows the scalar sum p_T of all tracks in the transverse region for jet data, compared with the PYTHIA Monte Carlo event generator. The average value of the scalar sum p_T of all charged tracks in the transverse region increases slowly with the leading E_T in the event, and is the same for jets and Z's, where leading jet $E_T \simeq p_{TZ}$. The integrals over all p_T of the curves in figure 4, when properly normalized, agree with the data points shown in figure 4.1 of Ref[1].

By definition the transverse region is relatively quiet, with most of the energy lying parallel to the thrust axis of the leading jet. The transverse region should be a good place to look for DPI, if one can devise a method to select events with jet activity there. This suggests a new technique to look for DPI: Use high p_T transverse tracks as a 'trigger' signature of a second hard interaction, by imposing the arbitrary requirement Σtranstrack$p_T > 15$ GeV/c as the trigger, and studying the jet activity in the transverse region of the 'triggered' events. Events with two separate vertices can be used to test the method.

4. Jet events with two vertices

The presence of more than one vertex per beam crossing depends on the luminosity, and on the definition of the second vertex. A total inelastic $\bar{p}p$ cross section of 60 mb at 1.96 TeV, [6] a luminosity of 1E32 cm^{-2}sec^{-1}, and a crossing frequency of 2.52 Mhz [7] gives and average $\bar{n} = 2.4$ interactions per beam crossing. Most of these secondary vertices are not detected with the criteria defined below, because they do not produce high p_T central tracks. The interaction region in the z direction at CDF was Gaussian, with $\sigma = 30$ cm, so that 2/3 of the interaction vertices were within ± 30 cm. The vertex resolution of the COT ($\sigma = 3$ mm) resolved 99% of the extra vertices. The primary vertex was the jet trigger vertex, with jet $E_T > 100$ GeV. The secondary vertex was defined as having at least 3 charged tracks with $p_T > 0.5$ GeV/c and $|\eta| < 1.$, separated from the primary vertex by at least 10 cm. For the data sample used, 30% of the events had a secondary vertex satisfying these requirements. From this number and the run averaged instantaneous luminosity of 1E32cm^{-2}sec^{-1} one obtains a cross section for the second vertex of $\sigma = 12$ mb. Figure 5 illustrates the procedure. The primary vertex, called vtx1 in the figure, has at least two jets, the highest E_T jet being the trigger, and the second vertex is at least 10 cm away. The transverse region defined on vtx1 is translated to vtx2, and the 'transverse tracks' are measured on vtx2. Tracks are used to define the vertices. A 100 GeV jet contains several charged particles, so the definition of the vertex is unambiguous. Assigning a vertex to a low E_T jet (10 GeV for example) is problematic, because there may be no tracks associated with the jet.

Figure 6 shows the scalar sum p_T spectrum of the transverse tracks on the second vertex, compared to the jet data shown in figure 4. Also shown is the fraction of transverse tracks with $p_T > 15$ GeV/c as a function of the E_T of the leading jet or Z.(The Z data are discussed below.) The fraction increases rapidly from 10^{-3} for 'minbias' to 10^{-2} for $p_{TZ} > 10$ GeV/c. Note that jet data and Z data agree. The 'trigger' creates a pair of jets on the second vertex with $E_T > 5$ GeV with a

Figure 3: Diagram showing the transverse region in the xy plane. The area shown in red is $\pi/3 < \Delta\phi < 2\pi/3$ relative to the leading jet or Z.
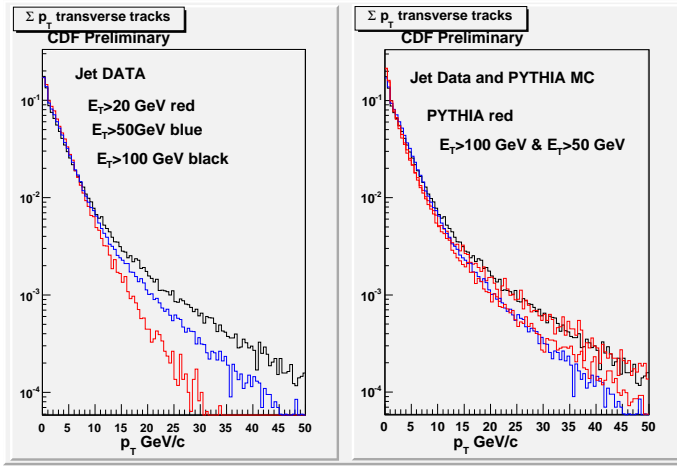
Figure 4: Scalar sum of p_T of transverse charged tracks for dijet data on the left, and compared to PYTHIA on the right. The fraction at $p_T > 15$ GeV increases with increasing jet E_T.

60% efficiency, so the overall probability of finding a pair of jets on the second vertex is 6×10^{-4}, or a dijet cross section of 7μb.

Figure 7 and figure 8 show the energies and azimuths of the jets created on the second vertex by the Σtranstrack$p_T > 15$ GeV/c 'trigger'. The extra jets appear in the transverse region in ϕ, just like they are supposed to. Their average energies are softer than those from the jet20 trigger - the lowest E_T CDF jet data sample. The key distribution is $\Delta\phi$ jets 3/4, shown in figure 9, which shows a clear back-to-back peak for the pair of independent jets created on the second vertex by the 'trigger'.

5. $Z \to \mu^+\mu^-$ **data sample**

The $Z \to \mu\mu$ final state was chosen for the DPI search because of its high purity and relative simplicity. The entire CDF run 2 muon data sample, $\int L \mathrm{dt} = 9\mathrm{fb}^{-1}$, was scanned to select $Z \to \mu^+\mu^-$ candidate events. The DPI search strategy was to use p_{TZ} to define the transverse region in ϕ. Only one vertex was allowed per event. The muon requirements were:

- Require two muons of opposite charge with $|\eta| < 1$. and $p_T > 20$GeV/c.
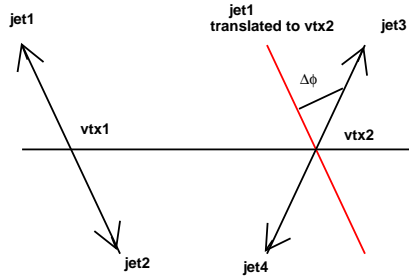
Figure 5: Diagram of the two vertex configuration. VTX1 is the primary vertex, where the 100 GeV trigger jet resides, and VTX2 is the secondary vertex, defined by at least three charged tracks with $p_T > 0.5$ GeV/c.
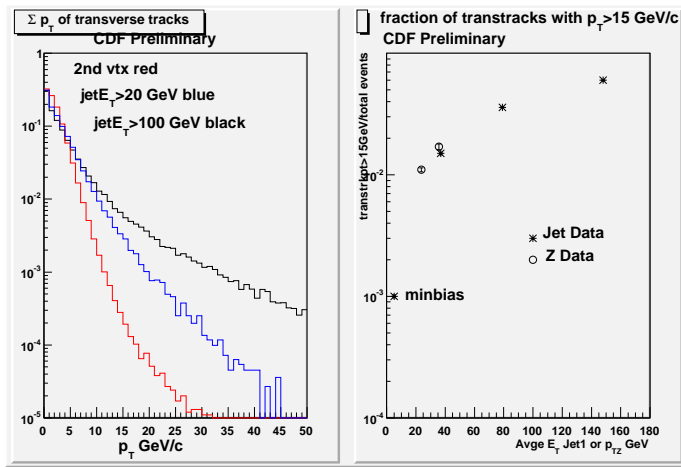
Figure 6: Left hand figure shows the scalar sum p_T of transverse tracks for the secondary vertex, compared to the same plots for jet20 and jet100. The secondary vertex is very soft, and is called 'minbias'. The right hand figure shows the fraction of events with scalar sum $p_T > 15$ GeV/c as a function of the highest jet E_T, or p_{TZ}. Note that the fractions for jets and Z's agree.

- Eliminate events with cosmic rays

- Require at least one good quality central muon satisfying CMU+CMP.

- 215589 events in $30 < m_{\mu\mu} < 130$ GeV mass range

- 176351 events in $80 < m_{\mu\mu} < 100$ GeV mass range - the Z's.

- 45633 events with at least one jet $E_T > 5$ GeV, and $p_{TZ} > 10$ GeV/c.

The resulting mass and p_T distributions for muon pairs are shown in figure 10, compared to the PYTHIA Monte Carlo including the CDF detector simulation. The agreement between the data and simulation is good. The simulation has a bit better mass resolution, and lies below the measured p_{TZ} distribution above 50 GeV/c.

Figures 11, 12, and 13 show the properties of the jet activity associated with Z events with $p_{TZ} > 10$ GeV/c, compared to the PYTHIA simulation.

6

6. Transverse region in Z production

Figure 14 shows the Σtranstrackp_T distribution for $p_{TZ} > 10 \mathrm{GeV}/c$, data and PYTHIA, and jet1 E_T distributions after the Σtranstrack$p_T > 15$ GeV/c 'trigger'. Figure 15 shows the effect of the 'trigger' on the azimuthal distributions of jets 1 and 2, both of which move into the transverse region. This is contrary to the expectations of DPI, where jet1, the highest E_T jet, is supposed to balance the p_{TZ}. In fact, both jets 1 and 2 shift so as to form a triangle to balance the Z, without any sign of DPI. This is shown in figure 16, where the 'trigger' has shifted the peak in $\Delta\phi$ jets 1-2 to about 2.3 radians, or $130°$, which just fits the vectors into a $120°$ triangle in the ϕ plane: $(\vec{p}_{TZ}, \vec{p}_{Tj1}, \vec{p}_{Tj2})$. Figure 16 also shows that $\Delta\phi$ jets 2-3 has no inhancement near π radians.

7. DPI search

If one assumes that there is one DPI of the type defined by the secondary vertex study, namely with three charged tracks $p_T > 0.5$ GeV/c, and $|\eta| < 1.$, in each Z production event with $p_{TZ} > 10$ GeV/c, then we expect $45633 \times 6. \times 10^{-4} = 27$ dijet events with a $\Delta\phi$ distribution like figure 9. Figure 9 is replotted in figure 17 normalized to 27 events, together with the observed $\Delta\phi$ jets 2-3 (352 events) for comparison.

An alternate estimation method is based on figure 6. The left hand plot shows that the scalar sum p_T of transverse tracks is not independent of the energies involved in the main collision. The energy dependence of the fraction $p_T > 15$ GeV/c increases monotonically with jet E_T or p_{TZ}. So the DPI contribution, if it exists, should be a decreasing fraction of the total as the E_T of the event increases. If one assumes that the Σtransversetrackp_T for Z's with $p_{TZ} > 10$ GeV/c contains within it a contribution from the DPI 'second vertex', then the fraction of the 352 dijets (2 & 3) coming from DPI would be $0.001/0.012 \times 352 = 29$ events, in agreement with the above estimate.

In order to place a limit on the probability of the DPI vertex from the curves in figure 17, it would be necessary to know with better accuracy the shape of $\Delta\phi$ 2/3 from the primary vertex.
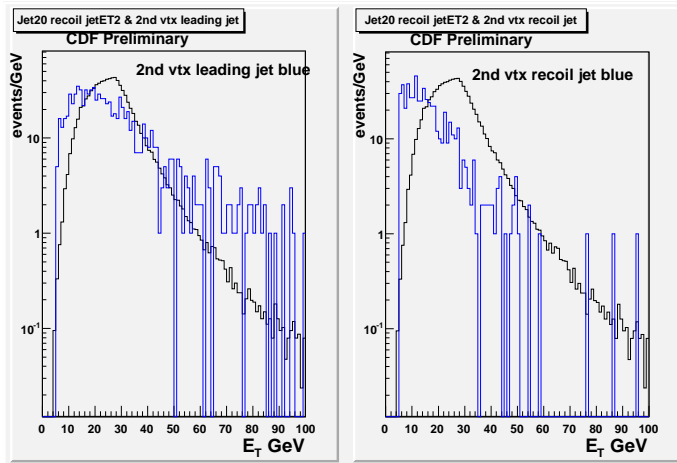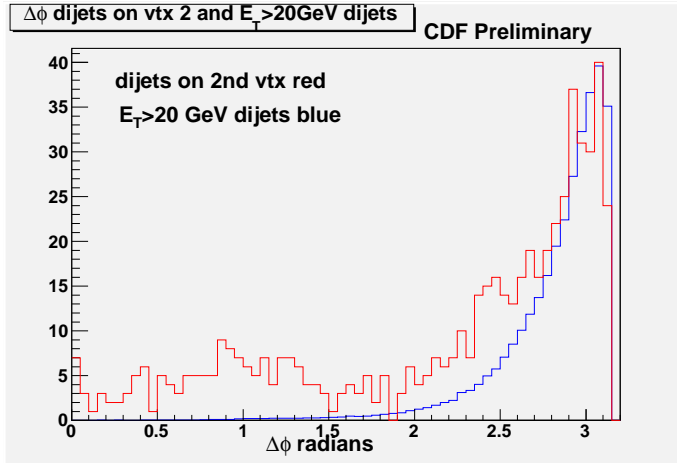

Figure 7: On the left is E_T for jet3, and right for jet4, created by Σtranstrack$p_T > 15$ GeV/c trigger on the second vertex. The energy distributions are compared to the recoil energy for a trigger jet $E_T > 20$ GeV. Jets 3 and 4 on average are softer than a jet20 trigger.
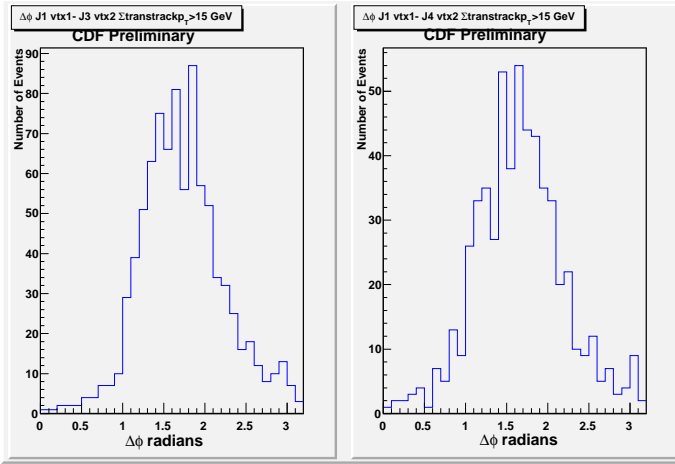
Figure 8: On the left is the azimuthal angle distribution of jet3 on vertex 2 relative to jet1 on vertex 1, and the same plot on the right for jet4 / jet1. The 'trigger' does what it is supposed to do: it creates jets in the transverse region in ϕ.
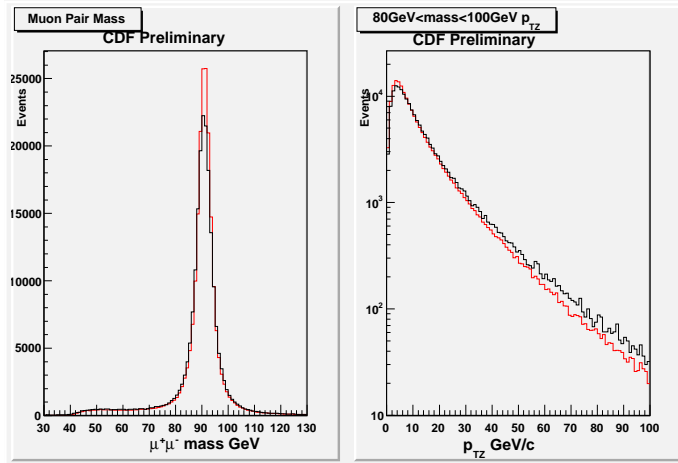
8. Acknowledgements

Figure 9: $\Delta\phi 34$ for the two jets on the second vertex created by the Σtranstrackp$_T > 15$GeV/c 'trigger'. The back-to-back peak is compared to that for jet20 dijets, which have larger average E$_T$, and hence better angular resolution.

Figure 10: Left hand plot shows the $\mu^+\mu^-$ pair mass data compared to PYTHIA Monte Carlo. The mass width for the data $\sigma = 3.8$ GeV is slightly larger than the Monte Carlo. The natural width is $\Gamma_Z = 2.5$ GeV. The right hand plot compared the p_{TZ} distributions in the Z mass range.
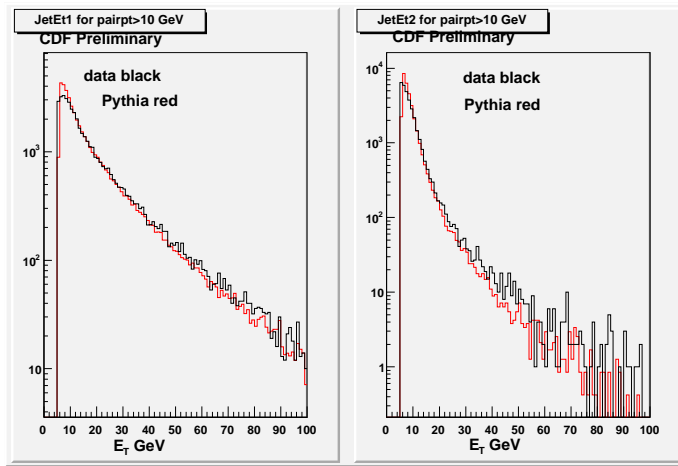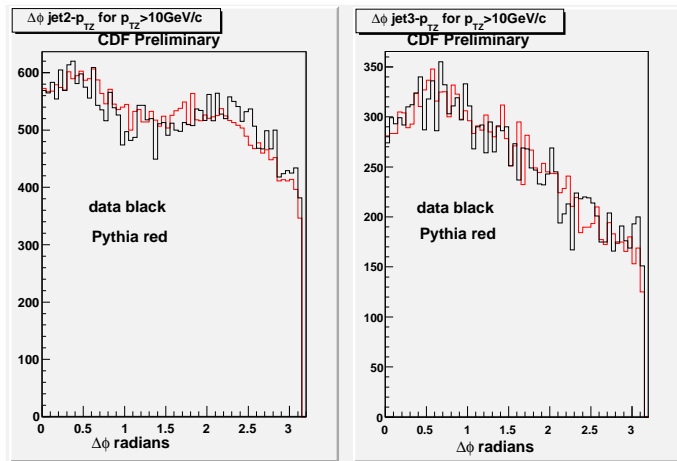

Figure 11: Left hand plot shows the recoil jet1 E_T distribution for $p_{TZ} > 10$GeV/c, data and PYTHIA. Right hand plot is the same for jet2. The jets are ordered in decreasing E_T.
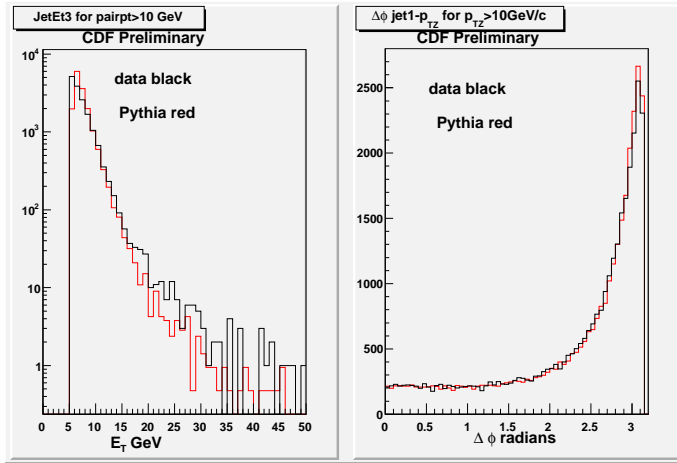
Figure 12: Left hand plot shows the recoil jet3 E_T distribution for $p_{TZ} > 10 \text{GeV}/c$, data and PYTHIA. Right hand plot is $\Delta\phi$ between jet1 and p_{TZ}. Note the strong recoil peak near $\Delta\phi = \pi$, and the long, rather flat tail.


Figure 13: Left hand plot is $\Delta\phi$ between jet2 and p_{TZ}, and the right hand plot is $\Delta\phi$ between jet3 and p_{TZ}, all for $p_{TZ} > 10 \text{GeV}/c$. PYTHIA agrees well with the data. The jets are not excluded from the transverse region.

PoS(Baldin ISHEPP XXI)001
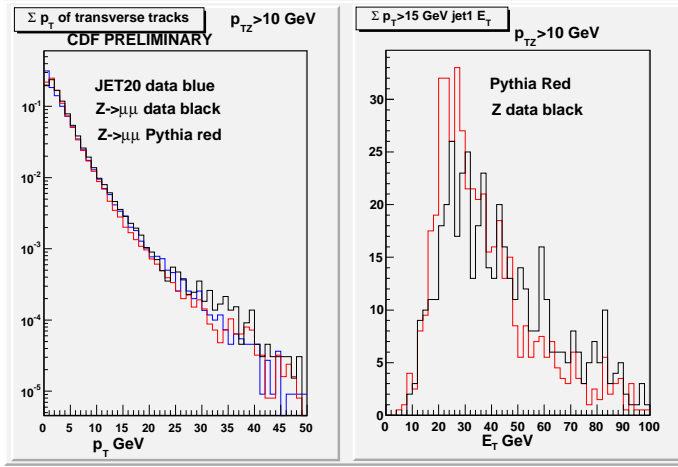
Figure 14: Left hand plot shows the Σtranstrackp_T distribution for $p_{TZ} > 10$GeV/c compared to jet20 data and PYTHIA Monte Carlo. The right hand plot is the leading jet E_T distribution after the Σtranstrack$p_T > 15$ GeV/c requirement.
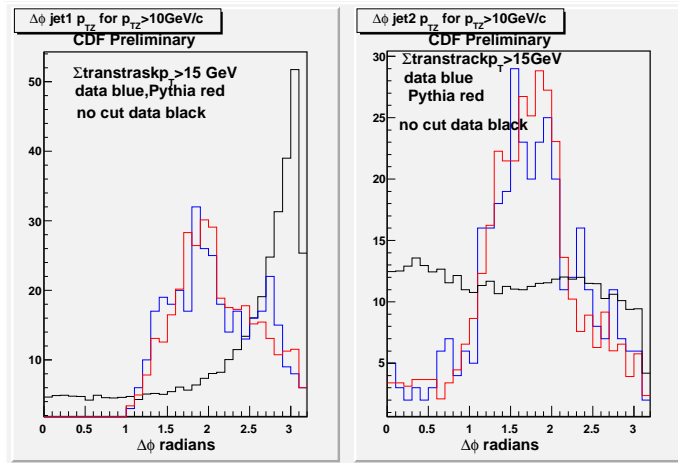
Figure 15: Left hand plot shows $\Delta\phi$ between jet1 and p_{TZ}, before and after the Σtranstrack$p_T > 15$ GeV/c cut, compared to PYTHIA. The right hand plot is the same for $\Delta\phi$ between jet2 and p_{TZ}. Note that both jets move into the transverse region.

11
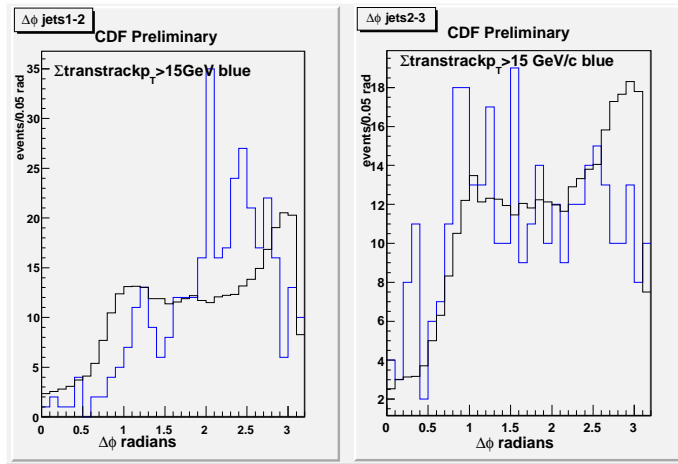
Figure 16: Left hand plot shows $\Delta\phi$ between jets 1 and 2 before and after the Σtranstrackp$_T$ > 15 GeV/c 'trigger' requirement. The before plot has been scaled by 0.011 to normalize to the same number of events. Note the peak in the after plot around 2.3 radians. The right hand plot is the same thing for jets 2 and 3. DPI should show up as a peak near π, where none is observed.
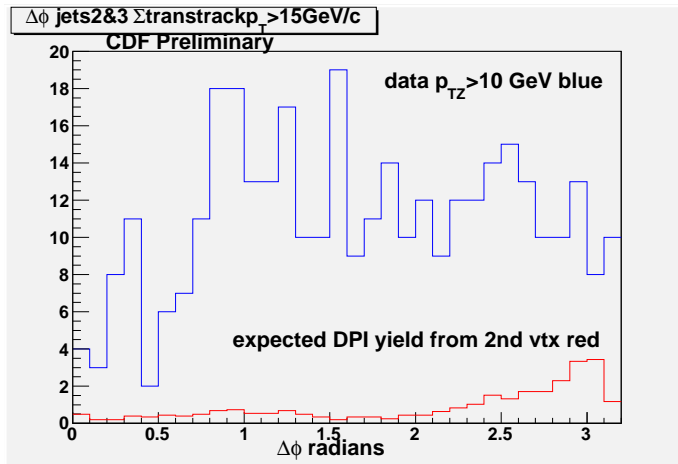
Figure 17: $\Delta\phi$ for jets 2-3 after the Σtranstrackp$_T$ > 15GeV/c compared to $\Delta\phi$ for jets 3-4 on the second vertex, normalized as described in the text. For DPI in the Z sample, one of the 'jets' is the Z, so jet1 is the recoil, and jets 2 and 3 form the independent scatter.

References

[1] T. Aaltonen *et al.,*(CDF Collaboration), Phys. Rev. D. **82,**034001 (2010).

[2] T. Sjostrand *et al.,* Comput. Phys. Commun. **135,** 238 (2001). This analysis used PYTHIA 6.2.2.4.

[3] V.M.Abazov *et al.,* (D0 Collaboration), Phys. Rev. D. **81** 052012 (2010).

[4] A. Abulencia *et al.,*(CDF Collaboration), J.Phys. G **34** 2457 (2007).

[5] A. Bhatti *et al.,*Nucl. Instr. Meth. A **566** 375 (2006).

[6] M.M.Block and F. Halzen, Phys. Rev. D 72, 036006 (2005). These authors quote a fitted total cross section at 1.8 TeV of 75 mb. Extrapolating to 1.96 TeV and subtracting the elastic cross section of 16 mb gives 60 mb inelastic.

[7] The bunch crossing frequency was constant during Tevatron Run 2. The peak luminosity was 4E32 $cm^{-2}sec^{-1}$, and 1E32 was fairly typical average over a 20 hour antiproton store.

PoS(Baldin ISHEPP XXI)001